Optical Detection and Characteristics of PCB Partial Discharge in More-electric Aircraft under Square Wave Voltage

Zang, Yiming ; Ghaffarian Niasar, Mohamad; Xu, Yongpeng ; Li, Ze; Qian, Qinglin ; Jiang, Xiuchen; Vaessen, Peter

DOI
10.1109/JESTPE.2024.3371010

Publication date
2024

Document Version
Final published version

Published in
IEEE Journal of Emerging and Selected Topics in Power Electronics

Optical Detection and Characteristics of PCB Partial Discharge in More-Electric Aircraft Under Square Wave Voltage

Yiming Zang, Mohamad Ghaffarian Niasar, *Member, IEEE*, Yongpeng Xu, Ze Li, Qinglin Qian, Xiuchen Jiang, and Peter Vaessen, *Member, IEEE*

***Abstract*— More electric aircraft (MEA) is an important direction for future aircraft development. The printed circuit boards (PCBs) of power electronics equipment in MEA operate in a complex environment of low air pressure, square wave voltage, compact layout, and strong electromagnetic interference, which makes the PCB more prone to partial discharge (PD). However, the effective detection method and related discharge characteristics for PCB PD under square wave voltage are still unclear. Therefore, this article proposes a PCB PD detection method based on fluorescent optical fiber, which has good anti-electromagnetic interference ability. The PD characteristics of the PCB with three typical structures under three air pressures are studied, including PD nonbreakdown characteristics, changes in optical pulse amplitude and pulse repetition rate during PD aging, PD breakdown path analysis, and PCB surface electric field simulation. The analysis shows that air pressure, space charge, and PCB surface flatness all have important influences on the PD of PCB under square wave voltage. It provides important theoretical support for the insulation protection design and fault diagnosis of PCB for MEA in the future.**

***Index Terms*— Discharge characteristics, more-electric aircraft, optical detection, partial discharge (PD), printed circuit board (PCB).**

I. Introduction

As THE demand for environmentally friendly aircraft gradually increases, more-electric aircraft (MEA) is one of the most important ways to replace traditional fuel-fired aircraft [1], [2]. The International Air Transport Association (IATA) has launched the international aviation industry's "2050 Net-Zero Carbon Emissions" announcement in 2021 [3]. The fuel-powered pneumatic aircraft limits their future development due to their high carbon emissions, complex on-board energy structure, and high flight costs, while MEA has the advantages of good environmental performance, lightweight structure, and high energy efficiency, which is the main trend of future aircraft development [4], [5].

The electrical energy-based drive system requires a large number of power electronics equipment in MEA, which makes printed circuit boards (PCBs) a critical part of supporting power electronics in MEA. Unlike conventional aircraft, PCB in the MEA is subjected to square wave voltage (or pulsewidth modulation voltage) generated by power electronics equipment, which can aggravate the aging of the PCB insulation [6], [7]. Moreover, the PCB in power electronics equipment of MEA has compact circuit structure and operates in a low-pressure environment, which makes the PCB more prone to partial discharge (PD) failure [8], [9], [10]. The PD failure can lead to serious shutdown of the MEA's electrical system, threatening flight safety. Thus, for reducing the risk of PCB PD, it is necessary to investigate the PD characteristics of PCB under square wave voltage, which can clarify the development process of PCB PD and guide the design of PCB insulation protection for power electronics in MEA.

Currently, some scholars have conducted studies related to PCB discharge and breakdown characteristics. Zhou et al. [11] studied the breakdown characteristics of PCBs in aircraft under the square wave pulse voltage and analyzed the failure mechanism. Yamada et al. [12] studied the breakdown characteristics of PCB under ac voltage and pulse voltage and compared the PCB surface images after the breakdown of different voltage waveforms. Meng et al. [13] studied the breakdown characteristics between PCB wires under different voltage conditions by changing the voltage parameters, such as pulsewidth, repetition frequency, and breakdown times of the pulse square wave, which provides suggestions for PCB electromagnetic compatibility design. Emersic et al. [14] investigated the PD aging characteristics and surface morphology changes of PCB under sinusoidal voltage. Most of the existing studies address the PD characteristics under sinusoidal voltage and breakdown characteristics of PCB under square wave voltage, while only few studies involve the PD characteristics of PCB under square wave voltage.

Regarding the PD detection of PCB in MEA, there are researches using pulse current detection and ultrahigh-frequency (UHF) detection to collect the PD signals of devices in MEA [15], [16], [17]. However, the above detection methods are easily subjected to electromagnetic interference from

Manuscript received 1 November 2023; revised 18 January 2024; accepted 16 February 2024. Date of publication 27 February 2024; date of current version 3 December 2024. This work was supported in part by the Startup Fund for Young Faculty (SFYF) at Shanghai Jiao Tong University (SJTU). Recommended for publication by Associate Editor Binbin Li. *(Corresponding author: Yongpeng Xu.)*

Yiming Zang, Yongpeng Xu, Ze Li, Qinglin Qian, and Xiuchen Jiang are with the Department of Electrical Engineering, Shanghai Jiao Tong University, Shanghai 200240, China (e-mail: zangyiming@sjtu.edu.cn; xyp3525@sjtu.edu.cn; lize123@sjtu.edu.cn; qianqinglin@sjtu.edu.cn; xcjiang@sjtu.edu.cn).

Mohamad Ghaffarian Niasar and Peter Vaessen are with the Electrical Sustainable Energy Department, Delft University of Technology, 2628 CD Delft, The Netherlands (e-mail: M.GhaffarianNiasar@tudelft.nl; P.T.M.Vaessen@tudelft.nl).

Color versions of one or more figures in this article are available at https://doi.org/10.1109/JESTPE.2024.3371010.

Digital Object Identifier 10.1109/JESTPE.2024.3371010

power electronics and square wave voltage in MEA, which makes it difficult to detect actual PD signals directly and accurately.

Therefore, in order to effectively detect the PD signal of PCB in the electromagnetic interference environment caused by square wave voltage, this article proposes an optical PD detection method based on fluorescent fiber. This method can immune to external electromagnetic interference, and the PD characteristics of PCB under square wave voltage can be obtained by detecting the optical radiation signal.

In this article, the PD behavioral characteristics of PCBs under square wave voltage with different PCB structures and different air pressures are investigated from the perspectives of the detection method, experimental phenomena, and mechanism analysis. It provides important theoretical support for PD protection and insulation design of PCB in MEA. The main contributions this article are as follows.

1) The optical detection method proposed in this article has excellent immunity to electromagnetic interference and high detection sensitivity, which is suitable for PCB PD detection under square wave voltage in MEA. Under different air pressure conditions, the distribution of phase-resolved PD (PRPD) patterns and the PD pulse delay phenomenon of PCB under square wave voltage are analyzed. The probability density distribution function of the PD optical pulse energy parameter is obtained. The correlation between optical and electrical PD pulses of PCB under square wave voltage at different air pressures is investigated.

2) For different air pressure environments, the change rule of optical pulse amplitude and pulse repetition rate during PD aging breakdown of PCB under square wave voltage is obtained. The reason for the change of optical pulse in the breakdown process is also analyzed theoretically.

3) The surface impurity deposition and breakdown channels of PCBs with different structures after PD aging breakdown are obtained by microscopic image observation. The effects of different PCB surface flatness on the surface electric field are analyzed by simulation, which provides an important reference for the insulation design and protection of PCB surface.

II. Fluorescent Fiber-Based PD Detection Technology and Experimental Setup

A. Fluorescent Fiber-Based PD Detection Principle

Different from traditional quartz fiber, fluorescent fiber has no limitation of the numerical aperture, which allows each position of the fluorescent fiber to receive optical radiation signals from any direction through the transparent cladding. The full-angle optical signal sensing way can capture PD optical signals radiated from each position of the PCB, which improves the effectiveness of PD detection.

The fluorescent fiber absorbs the light radiation signals of certain wavelengths through a doped fluorescent substance. When the fluorescent substance is excited by an external incident photon, the electrons in the fluorescent molecule leap from the ground state to the excited state. Since electrons are unstable in the excited state, they will jump to the ground state again and release fluorescence to the outside. When

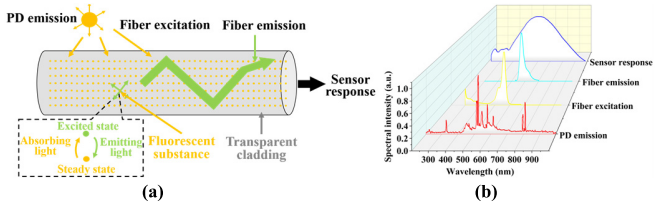

Fig. 1. Schematic of fluorescent fiber sensing principle. (a) Fluorescent fiber sensing process. (b) Spectral distribution.

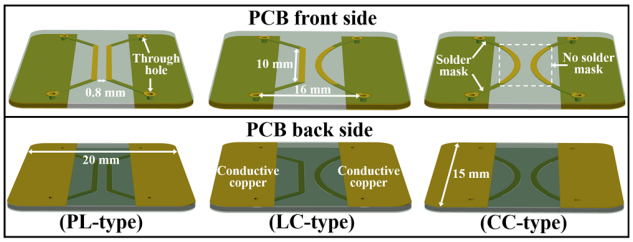

Fig. 2. Schematic of PCB structure (PCB type from left to right, named PL-type, LC-type, and CC-type).

the light generated by PD is incident on the fluorescent fiber, the light radiation generated by the excitation of the fluorescent substance satisfies the total reflection condition at the core–cladding interface. All the excited light propagates axially along the fluorescent fiber and finally be received by the optical sensor, as shown in Fig. 1(a).

For the fluorescent fiber-based detection method, the spectral distributions of the sensing parts need to match each other in order to effectively collect the PD optical radiation signals. The following two conditions need to be met.

1) The excitation spectrum of the fluorescent substance in the fluorescent fiber needs to cover the optical signal spectrum of the PD.

2) The emission spectrum of the fluorescent substance should be within the receiving spectrum of the optical sensor.

In this article, the above four spectral distributions are obtained based on experiments, references, and device manuals, which satisfies the above two conditions, as shown in Fig. 1(b).

B. PCB Design and Fabrication

In order to simulate the circuit layout of different PCBs, this article designs and makes three typical PCB track intersection types, specific dimensions, as shown in Fig. 2. The three PCB circuit layout structures are parallel linear (PL), linear-curve (LC), and curve–curve (CC). The three PCB types have conductors arranged on both the front and back sides, and the front and back sides of the PCB are connected by conductive through holes. There is a bare metal at the center area of the two tracks on the front of the PCB and at the two conductive coppers on the back, while the rest of the PCB is covered with a solder mask. On the front side of the PCB are two tracks for discharge. On the back side of the PCB are tow conductive coppers used for applying voltage and grounding in the experiment, respectively. The closest distance between the two tracks in each type of PCB is 0.8 mm, which meets the standard IPC 2221-A, the international test standard for PCB.

In addition, since the PCB in MEA is exposed to hazards from external factors, such as electrical, mechanical, radiation,

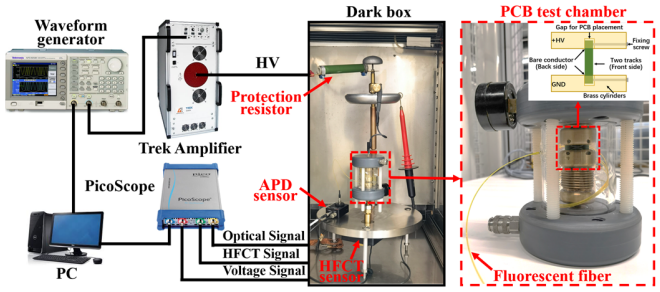

Fig. 3. PD optical detection experiment platform for PCB.

vibration, and so on, most of the PCB are covered with "conformal coating" on its surface to protect the PCB more stable operation. Based on the standard IPC-CC-830, silicone is a transparent insulating material with excellent protective properties and is now widely used as the conformal coating for PCB.

In this article, Silicone FSC-400 is used for making PCB's conformal coating. Silicone FSC-400 FSC is covered on the PCB surface by uniform spraying in a dry fume hood. After spraying, it is dried in an oven at 90° for 4 h. Although it is difficult to guarantee that the thickness of the conformal coating is exactly the same, the thickness of the coated PCB in this article is controlled between 30 and 50 μm, which has little effect on the experimental results. At least five or more PCBs of each structure are fabricated for experiment.

C. Experimental Platform Setup

An experimental platform is built in this article to carry out optical detection of PCB PD in MEA, as shown in Fig. 3. The test samples are placed in a transparent chamber capable of holding air pressure from 0 up to 10 bar. The PCB is fixed in a groove by means of insulating screws and is connected to the high-voltage source above and to the grounding electrode below by the conductive copper on the PCB back side. A fluorescent fiber is inserted in the transparent test chamber, which is used as a sensing element to receive the optical radiation signal generated by the PCB PD. Avalanche photodiode (APD) is used as an optoelectronic signal conversion device to collect the optical signal sensed by the fluorescent fiber and convert the optical signal into an electrical signal. At the same time, the HFCT sensor is used to synchronously collect the PD electrical signal of PCB for comparative analysis. A high-voltage probe is used to record the voltage waveform applied to the PCB. The PCB test chamber, the high voltage side, and the PD detection system are placed in an incompletely dark box. A PicoScope oscilloscope is used to synchronize the acquisition of optical signals, HFCT signals, and voltage signals. Due to the material properties of the fluorescent fiber itself, compared with HFCT detection and UHF detection, it has good anti-electromagnetic interference capability and can be well adapted to the PD detection of PCB in MEA under square wave voltage.

The bipolar square wave voltage is generated by a computer-controlled arbitrary waveform generator and amplified by a Trek 30/20A power amplifier. The square wave voltage frequency is 400 Hz, which is the typical frequency of the power system voltage in the MEA [2]. The voltage duty cycle is 0.5. Limited by the lack of fast square-wave voltage source equipment in the laboratory, the dV/dt of the applied voltage in this article (550–1000 V/μs) is relatively slower than that of fast square wave voltages in actual power electronics, such as PWM voltages. However, by analyzing the experimental phenomena and referring to the existing reference, the study of PCB PD at microsecond-level square wave voltages can also characterize and interpret most of the PCB PD phenomena at nanosecond-level square wave voltages. Therefore, regarding the two aspects of PD signal detection and insulation characteristics, which are the focus of this article, the voltage applied in this article can adequately carry out the related research.

In this article, three air pressure environments are set up, namely, one time of atmospheric pressure (1 atm), 0.5 atm, and 0.1 atm. Each PCB structure is subjected to PD experiments at the three atmospheric pressures. During the PD experiment, the voltage is slowly increased to the inception voltage of PD (PDIV). Since the PDIV is different under different experimental conditions and the PD phenomenon is not stable enough at the PDIV, the PD experiments are conducted by applying 1.1 times the PDIV (1.1 PDIV) to the PCB in each condition until breakdown.

III. Results and Discussion of Nonbreakdown Experiment

This section introduces the pulse characteristics and signal distribution of the PCB during the PD nonbreakdown process and provides the theoretical characteristic reference for the PD detection of the PCB in MEA. The PRPD pattern, PD pulse delay distribution, probability density distribution of PD pulse intensity, and PD optical–electrical pulse relationship of PCB are obtained and analyzed.

A. PRPD Patterns and PD Pulse Delay Distribution

The PRPD pattern can describe the distribution of PD pulses in the phase and is a typical statistical feature that can reflect the discharge state. In order to explore the influence of different air pressures and PCB track structure on the phase distribution of PCB PD, the PRPD patterns of the above three PCB structures under 1-, 0.5-, and 0.1-atm air pressure are studied, as shown in Fig. 4. Each PRPD pattern contains 1000 PD pulses.

In Fig. 4, the green area represents the density distribution of the PD data points. The square wave voltage changes polarity at 0° and 180° phase. From Fig. 4, it can be obtained that the phases of the PCB PD under the square wave voltage are mainly distributed at the rising edge of the square wave voltage, especially under the air pressure of 1 and 0.5 atm. This phenomenon is mainly determined by the external electric field, space charge, and the source of the initial electrons. The emission from the PCB surface or the initial electrons in the air is the prerequisite for the PD generation. When the first PD occurs, some space charges can be deposited on the surface of the PCB, and the electric field formed by these space charges is opposite to the external electric field. When the polarity of the square wave voltage is suddenly reversed, the deposited

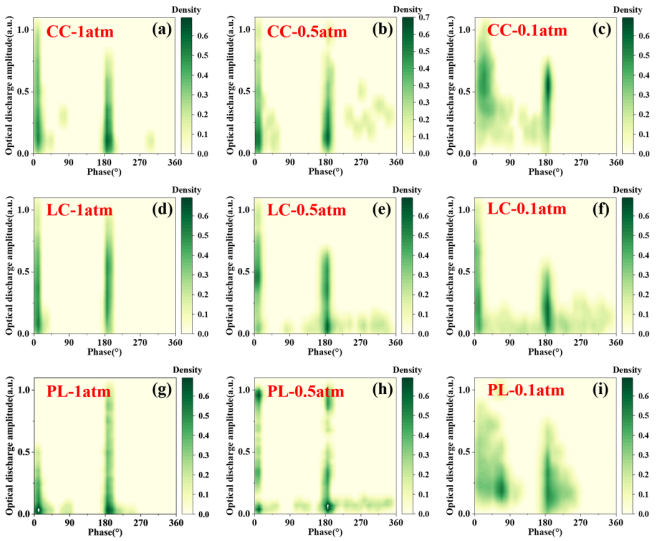

Fig. 4. PRPD patterns of three PCB structures under three air pressures. PRPD patterns of PCB with [(a)–(c) CC-type structure at 1, 0.5, and 0.1 atm, (d)–(f) LC-type structure at 1, 0.5, and 0.1 atm, and (g)–(i) PL-type structure at 1, 0.5, and 0.1 atm].

space charge increases the net electric field strength on the PCB surface, making PD more likely to occur and larger in magnitude.

However, as the air pressure decreases, the phase distribution of the PD becomes wider. More discharges appear in the PRPD patterns of the three PCB structures within 0°–180° and 180°–360°, not only mainly concentrated around 0° and 180°. This shows that the reduction of the air pressure causes the PD to occur at the phase which is difficult to discharge under atmospheric pressure.

In order to better analyze the influence of air pressure on the PD delay characteristics, this article counts the time interval between the occurrence of PD pulses and the change of square wave voltage polarity under different air pressures. Since the PCBs of these three structures all have similar delay characteristics, the PCB with PL-type structure is used as an example for illustration, as shown in Fig. 5. Under three air pressures, taking the rising edge of the positive polarity and negative polarity square wave as the time reference, the PD pulse time delays under the positive and negative square wave voltages are calculated, respectively. The zero-crossing position of the square wave voltage is the starting point for delay time calculation.

In Fig. 5, it is observed that as the air pressure decreases, a long-delayed discharge occurs at both positive and negative polarities of the square wave voltage. Especially at 0.1-atm air pressure, there are more than 20 pulses with a delay of more than 313 μs. There is also a new interesting phenomenon. As the air pressure decreases, there is a tendency for the PD to occur with shorter delay after the polarity change of the square wave voltage, which means that the PD is generated earlier during the rising of the square wave voltage, for both positive and negative polarities.

Both of these phenomena are closely related to the generation, migration, and dissipation of space charge. According to the typical volume–time (V–T) discharge theory, the probability of a PD occurring can be expressed as a function of

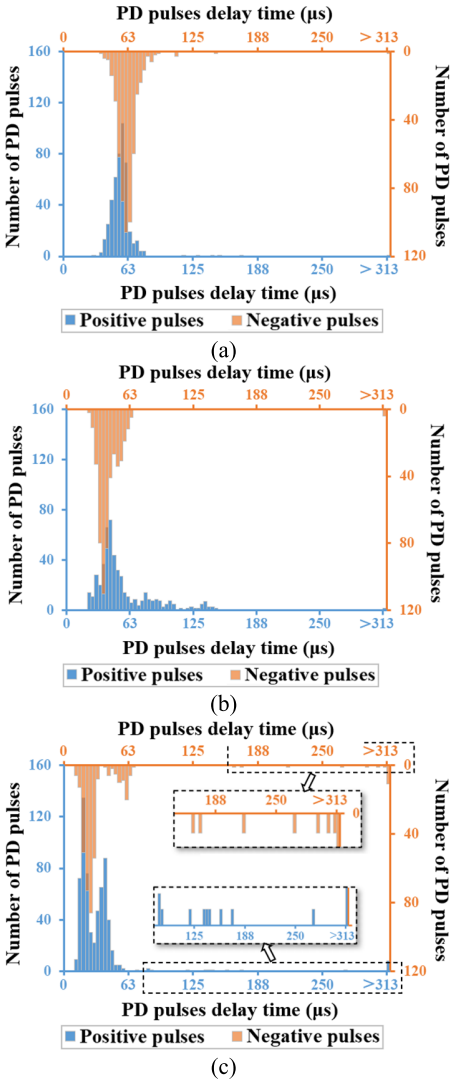

Fig. 5. PD pulses delay time distribution under different air pressures. (a) 1 atm. (b) 0.5 atm. (c) 0.1 atm.

the electrode shape, gas pressure, and voltage waveform [18], [19], [20]. Although the V–T theory is initially proposed at sinusoidal voltages, it is also applicable to the phenomenon of short-term PDs at square wave voltages [21]. The V–T model calculates the probability of generating a critical avalanche within a critical volume by means of a Weibull distribution function

$$P = 1 - \exp\left[-\int_0^t \left(\int_{V_{cr}} \frac{dn}{dt}\left(1-\frac{\eta}{\alpha}\right)dV + \int_{S_{cr}} \frac{di}{dt}\left(1-\frac{\eta}{\alpha}\right)dS\right)dt\right] \quad (1)$$

where V_{cr} is the critical volume, S_{cr} is the critical surface, dn/dt is the rate of electron detachment within the critical volume, di/dt is the rate of electron detachment form the critical surface, α is the ionization coefficient, η is the attachment coefficient, and critical volume and critical surface are the range within which there is sufficient electric field strength to excite electron avalanches.

The above rate of electron detachment within the critical volume dn/dt and the rate of electron detachment di/dt can be

expressed as follows [22], [23]:

$$\frac{dn}{dt} = \frac{E}{E_{cr}} \times n^{-} \tag{2}$$

$$\frac{di}{dt} = \frac{e^3(\beta E)^2}{8\pi h(e\varphi_D)} \exp\left(-\frac{8\pi\sqrt{2m}}{3he\beta E}(e\varphi_D)^{\frac{3}{2}}\right) \tag{3}$$

where E is the electric field, E_{cr} is the critical electric field, n^{-} is the negative ion number, e is the electron charge, β is the field factor, h is Planck's constant, φ_D is the potential barrier height, and m is the effective electron mass.

The effective ionization coefficient (α-η) is a function of air pressure p and electric field E, and some studies have obtained some empirical formulas, for example [24]

$$\frac{\alpha-\eta}{p} = 0.161\left(\frac{E}{p} - 21.65\right)^2 - 2.87. \tag{4}$$

Based on the above, all the parameters in (1) of the V–T theory are related to the air pressure and the electric field, which means that the probability of generating a discharge can be explained by the changing of air pressure and electric field. Since the applied voltage is the same 1.2 PDIV on each PCB, the air pressure has a greater effect on the PD pulse time delay compared to the electric field.

When the air pressure decreases, the negative ions in the air on the surface of the PCB are reduced. According to (1) and (2), the decrease in negative ions can result in a corresponding diminishing in the rate of electron detachment, which requires the electric field to be applied for a longer period of time to increase the probability of discharge [24]. This is reflected in the statistical result that the PD pulse in Fig. 5 shows a significant time delay at low air pressure.

In addition, as the air pressure decreases, the probability of collision between electrons and gas molecules decreases, increasing the mean free path and collision velocity of electrons. Therefore, accelerated by relatively lower electric field strength, free electrons can collide to produce new electrons to satisfy the critical effective ionization coefficient, thus promoting the discharge probability. As a result, the lower the air pressure in Fig. 5, it is observed that PD near the rising edge of the square wave voltage appears earlier, and even some discharges are generated before the rising edge fully reaches the peak of the square wave voltage.

B. Probability Density Distribution of PD Optical Pulse Intensity

The PD pulse intensity characteristics of PCB under square wave voltage are an important reference for PCB insulation design and PD diagnosis. Thus, the probability density distributions of PD optical pulse amplitude and PD optical pulse energy are explored in this article.

The PD optical pulse data of each PCB structure under three gas pressures are collected for probability density distribution analysis. Each probability density distribution statistical sample contains 1000 consecutive PD optical pulses. For PD statistical parameters, the amplitude of PD optical pulses (P_1), the average value of every 10 PD optical pulses (P_2), the energy of PD optical pulses (P_3), and the maximum energy value of every 10 PD optical pulses (P_4) are calculated. The amplitude parameter (P_1 and P_2) of the PD optical pulse can be recorded directly through the data. P_3 is calculated as follows:

TABLE I
R-SQUARE RESULT FOR DIFFERENT PROBABILITY DISTRIBUTIONS

Parameters	Lognormal	Gauss	Voigt	Giddings	Lorentz
P_1	0.9583	0.9315	0.9330	0.8726	0.9172
P_2	0.9573	0.9483	0.9500	0.6324	0.9402
P_3	0.9618	0.9078	0.9175	0.9438	0.9103
P_4	0.9432	0.9084	0.9093	0.9093	0.9009

$$P_3 = \int_{t_{10\%}}^{t_{90\%}} A(t)dt \tag{5}$$

where $t_{10\%}$ and $t_{90\%}$ are the time of the PD optical pulse at 10% amplitude and 90% amplitude, respectively, and $A(t)$ is the function of the complete waveform of the PD optical pulse. P_4 can be obtained by calculating the maximum value of every 10 P_3. The Lognormal, Gauss, Voigt, Giddings, and Lorentz probability distributions are used to fit the above four parameters, and the R-square values of each probability distribution are calculated to measure the quality of different fitting functions. The experiment found that the PCB structure has little effect on the probability distribution, so one PCB structure is chosen to calculate the average R-square value for each probability density distribution at three air pressures, and the results are shown in Table I. Lognormal has the maximum R-square value for each PD statistical parameter, so the Lognormal function is chosen to describe the probability density distribution of PD pulse intensity. The probability density function (pdf) of Lognormal is expressed as

$$f(x) = \frac{1}{x\sigma\sqrt{2\pi}} \exp\left(-\frac{(\ln x - \mu)^2}{2\sigma^2}\right) \tag{6}$$

where x is the PD statistical parameter, and σ and μ are the expected value and standard deviation of the parameter's natural logarithm, respectively.

The cumulative distribution function (cdf) of Lognormal is the integral of (6)

$$F_c(x) = \Phi\left(\frac{(\ln x - \mu)}{\sigma}\right) \tag{7}$$

where Φ is the cumulative distribution function of the standard normal distribution.

According to the above analysis, a typical sample is selected to plot the pdf and cdf of four PD statistical parameter, as shown in Figs. 6 and 7. In Fig. 6, the pdf distribution shape of the P_1 parameter has the characteristic of deviating to low amplitude, which shows that the PCB has more small-amplitude PD optical pulses when the PD is stable. Differently, the pdf of the P_2 parameter has better symmetry, which means that it is rare for ten consecutive PD optical pulses to be particularly small amplitude or large amplitude. This suggests that it is necessary to collect and analyze several consecutive pulses before and after as much as possible, so as to obtain the real and typical PD state. In Fig. 8, the pdf distribution of the P_3 and P_4 parameters is similar to the

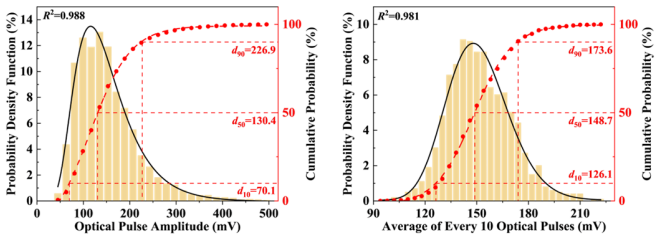

Fig. 6. Probability density distribution of PD optical pulse amplitude parameters (P_1 and P_2).

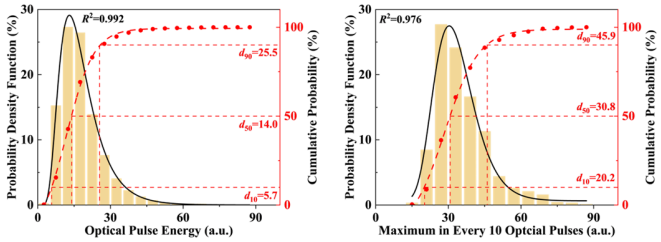

Fig. 7. Probability density distribution of PD optical pulse energy parameters (P3 and P4).

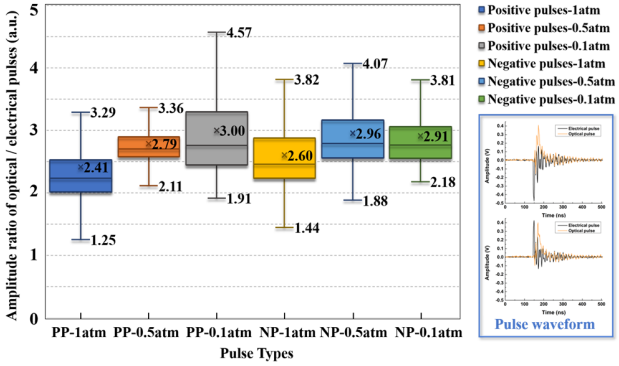

Fig. 8. Optical–electrical pulse amplitude ratio of PCB PD under different air pressures.

distribution shape of the P_1 parameter, indicating that the maximum energy value in several consecutive PD pulses can roughly reflect the intensity distribution of the current PD pulses.

Since there are a few actual detection samples of PCB PD in MEA, based on the above probability density distribution function, a small number of samples can be used to fit and predict more complete PD pulse amplitude and energy distribution, providing important support for PCB factory quality monitoring and fault diagnosis in the future.

C. PD Optical–Electrical Pulse Relationship

Optical detection has obvious advantages in PCB PD detection under square wave voltage due to its excellent anti-electromagnetic interference ability and high sensitivity. Since PCB in MEA usually operates in a low-pressure environment, changes in air pressure have a certain impact on photon propagation. Therefore, the variation of the amplitude ratio of the optical signal to the electrical signal under different air pressures is studied, as shown in Fig. 8. Each pulse type in Fig. 8 contains 1000 ratio data, and each ratio data is the average value of the ratios of three PCB structures under this air pressure.

The PD electrical pulse detected by HFCT has positive pulse (PP) and negative pulse (NP), so the absolute value of the NP is used for calculation. The PD photon radiation detected by the fluorescent fiber only has PP, as shown in the pulse waveform in Fig. 8. It can be seen from Fig. 8 that the amplitude ratio of optical/electrical PD pulses tends to increase as the air pressure decreases, both for positive and negative electrical pulses. This phenomenon shows that low air pressure can reduce the attenuation of PD optical radiation signal and improve the effectiveness of detection.

Since the reduction in pressure decreases the density of gas molecules around the PCB, the number of molecules participating in photoionization process decreases. However, the light radiation generated by ion recombination during the discharge process remains at a high level under low pressure, which makes more photons radiate without participating in the photoionization process, resulting in more photons being detected. This may be the reason why the optical/electrical amplitude ratio of PD increases under low pressure. The specific principles should be further confirmed in the future. It is indicated that the optical detection method is very suitable for PD detection of equipment operating in a low-pressure environment, such as MEA.

IV. Results and Discussion Of PCB Aging Breakdown Characteristics

The breakdown process of PCB under PD in MEA is an important reference for PCB insulation tolerance and fault state diagnosis. In this section, the changing rules of PD optical pulse amplitude and PD optical pulse repetition rate of PCB from the PD generation to the breakdown process are investigated.

A. PD Optical Pulse Amplitude During Aging Breakdown

In the experiments, the samples of all three PCB structures are subjected to PD aging breakdown experiments in three air pressure environments (1, 0.5, and 0.1 atm), respectively. The breakdown time of different PCB samples varies greatly, and it may differ by more than 1 h. In this article, the overall aging breakdown time of each PCB sample is divided into ten time points, and the average value of 10 000 consecutive PD optical pulse amplitudes at these ten time points is counted as the PD aging data. Then, the PD aging data (PD optical pulse amplitude) of each structure are normalized to [0, 1]. Finally, the normalized data of the three PCB structures under the same air pressure are added up to obtain the changing rule of PCB PD optical pulse amplitude under one air pressure in Fig. 9.

In Fig. 9, the variation of PD optical pulse amplitude and HFCT pulse amplitude during the aging breakdown process shows an overall trend of decreasing and then increasing, which is divided into three stages. The trends of the optical pulse amplitude and the HFCT pulse amplitude are basically similar in Stages 1 and 3. In Stage 3, there is a certain degree of fluctuation in the change of optical pulse amplitude and HFCT pulse amplitude, but the overall trend is basically similar. This also indirectly proves that there is a certain correspondence

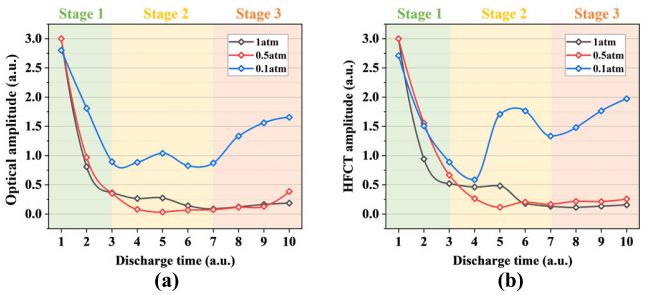

Fig. 9. (a) Optical pulse amplitude and (b) HFCT pulse amplitude during PD aging breakdown under different air pressures of PCB.

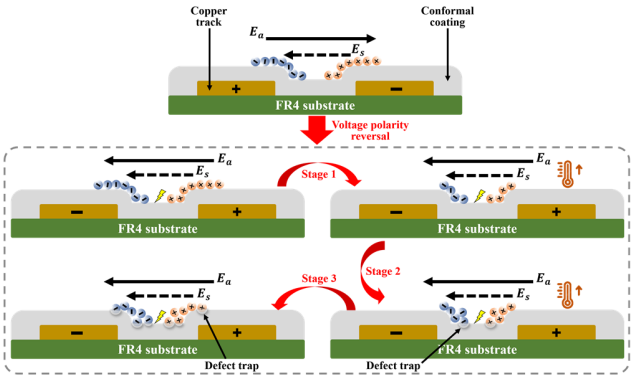

Fig. 10. Surface charge evolution process and discharge principle during PCB PD breakdown.

between the optical detection method and the HFCT detection method, which provides the feasibility of the subsequent PD severity assessment by optical detection.

The schematic of PCB surface space charge change and discharge principle in three stages in Fig. 9 is shown in Fig. 10 and explained as follows.

For stage 1: According to the analysis in Section III, most of the PD under the square wave voltage is concentrated when the voltage polarity is reversed. The electric field formed by the space charge on the PCB surface can increase the electric field intensity generated after the voltage polarity is reversed. The greater the accumulation of space charge, the greater the superimposed discharge electric field, resulting in a larger PD optical pulse amplitude. However, the PD under the square wave voltage can cause local heating on the PCB surface, which increases the surface conductivity of the silicone rubber on the PCB, thereby accelerating the dissipation of surface space charges [25]. Therefore, as the accumulated surface charge decreases, the superimposed electric field also decreases, and finally, the PD discharge intensity gradually decreases.

For stage 2: As the PD aging progresses, defects, such as cracks, crystals, holes, or flocs, begin to appear on the PCB surface, which can form traps to limit the dissipation of surface charges. At the same time, due to the external heat exchange, the surface temperature of the PCB rises to a certain temperature under the action of PD and then tend to be stable. Therefore, the dissipation rate of the PCB surface charge decreases, making the discharge intensity tend to be stable.

For stage 3: After a relatively long period of PD aging, the number of defect traps on the PCB surface gradually increases,

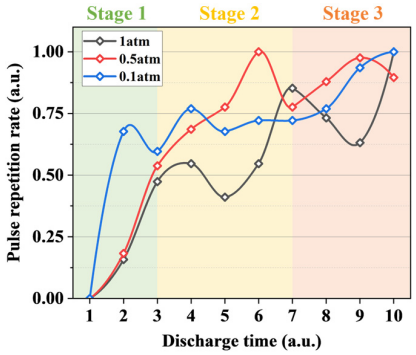

Fig. 11. Optical pulse repetition rate during PD aging breakdown under different air pressures of PCB.

and the limiting effect on surface charge dissipation begins to gradually outweigh the promoting effect of temperature rise (temperature rise will stabilize). The PCB surface charges begin to accumulate and increase, thereby increasing the superimposed electric field during discharge. Meanwhile, long-term PD also reduces the insulating properties of the surface conformal coating and increases the electric field strength between the electrodes. Therefore, the PD discharge intensity shows an upward trend at all three air pressures. Especially at 0.1 atm, since the insulation strength of the air on the surface of the PCB is lower, the increase of the PD intensity is relatively more obvious.

B. PD Optical Pulse Repetition Rate During Aging Breakdown

Based on the experimental recording method in Section IV-A, the PD optical pulse repetition rate in each case is recorded synchronously, as shown in Fig. 11. According to the division of the three stages in Fig. 9, it is found that there is no obvious stage difference for the PD optical pulse repetition rate, but the overall pulse repetition rate tends to increase as PD aging proceeds. The PCB PD all first occur near the fast-rising edge of the square wave voltage, while the frequency of the square wave voltage remains unchanged, indicating that the increase in the pulse repetition rate is mainly due to the increased discharge of the square wave voltage in the dc phase. This phenomenon is mainly affected by the electron generation rate on the PCB surface.

The electron generation rate in the PCB PD process is mainly determined by background ionization, surface emitted electrons, and electron detachment [26], which is expressed as follows:

$$N(\dot{E}) = N_0 + N_d + N_F(\dot{E}) \tag{8}$$

where $N(\dot{E})$ is the electron generation rate, N_0 and N_d are the electron change rate by background ionization and detachment, respectively, and $N_F(\dot{E})$ is the electron change rate by surface emission. Under square wave voltage, $N_F(\dot{E})$ of PCB PD can be expressed as a function of electric field E

$$N_F(\dot{E}) = N_0 \exp\left[-\left(\frac{1}{\tau}\right)\right] \exp\left|\frac{E}{E_{\text{inc}}} \cdot \frac{T_{\text{sur}}}{T_{\text{amb}}}\right| \tag{9}$$

where τ is the time constant associated with the discharge time delay, E_{inc} is the inception discharge electric field, T_{sur}

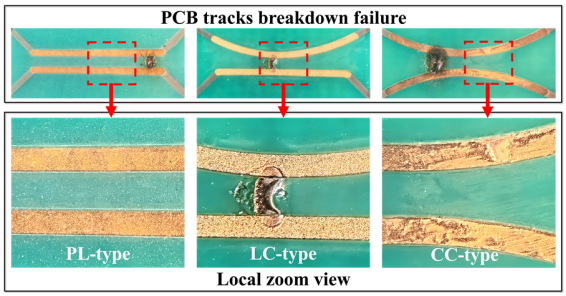

Fig. 12. Overall and local view of PD breakdown on PCB surface.

is the PCB surface temperature, and T_{amb} is the ambient air temperature.

According to (8) and (9), the PCB surface temperature rising and surface degradation during PD aging can promote the surface emission of electrons and the detachment of electrons, resulting in an increase in the electron generation rate. The increase of the electron generation rate correspondingly increases the probability of PD generation, so that the PD optical pulse repetition rate increases with the aging of the PD in Fig. 11. In addition, the impact of the previous PD on the background ionization of the subsequent PD is relatively random, which also leads to certain fluctuations in the pulse repetition rate in Fig. 11. Based on this phenomenon, the PD optical pulse repetition rate can be used to provide a reference for the PCB PD severity evaluation in MEA.

V. PCB Breakdown Fault Results and Simulation Analysis

In this section, the surface failure morphology of three PCB structures after breakdown is investigated, and the effects of PCB surface bumps and dents on the electric field distribution are studied by COMSOL simulation, which provides a theoretical basis for the PCB insulation design and the conformal coating preparation.

A. PCB Breakdown Failure Results

After the PD aging breakdown experiments of the PCB, the breakdown paths and the PCB surface condition of the three PCB structures are observed, as shown in Fig. 12.

As can be seen in Fig. 12, the PCB of the LC-type and CC-type structures does not breakdown as expected at the location, where the copper tracks are closest to each other, but rather a penetrating breakdown occurs at a location, where the two copper tracks are relatively far apart. The heat generated during the breakdown process caused the conformal coating around the breakdown path to melt. This relatively random breakdown phenomenon presents a greater challenge to the design and protection of PCB insulation. In addition, white tiny powdery impurities are found to be deposited in the unbroken areas of the PCB surface, especially around the copper tracks. These deposited impurities are probably attracted to the PCB's electrodes due to the polarization that occurs during the prolonged discharge process.

B. PCB Surface Electric Field Simulation Characteristics

Currently, most of the PCB conformal coating is fabricated by spraying and dipping, which can lead to ripples or other

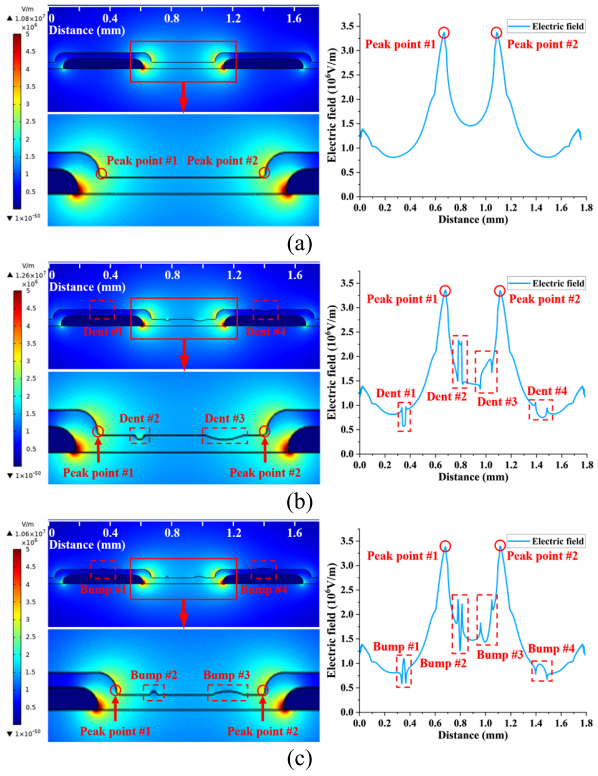

Fig. 13. PCB electric field distribution under different surface conditions. (a) Flat PCB surface conformal coating. (b) PCB surface conformal coating with dents. (c) PCB surface conformal coating with bumps.

unevenness on the conformal coating surface after solidification. By analyzing the breakdown phenomenon, the flatness of the PCB conformal coating should be one of the reasons for the random PCB breakdown location. Thus, in this section, the effect on the surface electric field when there are bumps and dents on the PCB surface conformal coating is simulated and analyzed in COMSOL software.

According to the structural size and conformal coating type of the PCB in this article, a corresponding 2-D simulation model of the PCB cross section is built in COMSOL. The copper track on the one side of the PCB is applied with a voltage of 2 kV, and the other side is grounded. In order to simulate the PCB conformal coating with different surface flatnesses, bumps and dents of different sizes are set above copper tracks and between two copper tracks. The electric field distribution of the conformal coating top surface under different surface conditions is obtained by the simulation. The electric field peaks on the PCB surface and the electric field distribution of dents and bumps areas are specially marked, as shown in Fig. 13.

According to the simulation result, it is found that the peak values of the electric field distribution under different PCB surface conditions are at the triple junction of the copper track, conformal coating, and substrate, which is the key area of insulation protection.

For the conformal coating surface with dents, when the dent is located between two copper tracks, the presence of the dent causes a localized enhancement of the electric field to appear. The smaller the curvature radius of the dent, the more pronounced the local distortion of the electric field, which

is caused by the bottom geometry of the dent being more susceptible to charge accumulation. When the dent is located above the copper track, the electric field strength of the dent surface is relatively lower, which is because the dent surface is farther away from the electric field distortion region.

For the conformal coating surface with bumps, when the bumps are located between two copper tracks, a distortion of the surface electric field is caused by the bump. Since the geometry at the bottom of the bump is more irregular than at the top, the electric field strength increases at the bump bottom. At the top of the bump, the electric field strength is relatively reduced. When bumps are located above the copper tracks, the presence of the bump causes the electric field strength to increase, in contrast to the effect of the dent.

According to the above simulation results, it can be indicated that the flatness of the conformal coating has an important influence on the electric field distribution on the PCB surface. The uneven conformal coating increases the risk of local breakdown, which also provides a reasonable explanation for the randomness of PCB breakdown locations. Therefore, the PCB conformal coating surface in the MEA should be made smooth and flat to ensure the reliability of the insulation.

VI. Summary and Conclusion

Based on the optical detection method, the PCB PD characteristics with three structures under square wave voltage are studied at three air pressures, and the influence of PCB surface flatness on the electric field distribution is also investigated by COMSOL simulation, which provides theoretical support for PD detection and insulation protection design of PCBs in MEA. The research results are summarized as follows.

1) A PCB PD detection method based on fluorescent optical fiber is proposed, which can effectively overcome the electromagnetic interference during the PCB operation in MEA and improve the effectiveness of PD detection. Besides, the flexibility of the optical fiber is beneficial for its arrangement in the equipment, which is an effective way for the PD detection of PCB or other electrical equipment in the MEA in the future.

2) For the nonbreakdown PD characteristics of PCB under square wave voltage, it is mainly related to air pressure and has little correlation with the PCB structure. As the air pressure decreases, the PRPD pattern distribution of the PCB under the square wave voltage gradually becomes wider, and PD pulses appear to be significantly delayed. The ratio of PD optical/electrical pulse amplitudes gradually increased with decreasing air pressure. However, the probability density distribution of PD optical pulse intensity is basically the same under different air pressures and different structures, which basically satisfy the Lognormal distribution.

3) For the PCB aging breakdown characteristics under square wave voltage, the optical pulse amplitude of PCB PD presents three-stage characteristics of decreasing first, then stabilizing, and finally rising slowly as PD aging progresses, which is mainly affected by the space charge distribution on the PCB surface. In addition, the optical pulse repetition rate of PCB PD gradually increases with PD aging, but there are certain fluctuations, which is mainly caused by the increase of effective electron generation rate.

4) For the three typical PCB structures, the PD aging breakdown path under square wave voltage is not located at the closest position of the PCB copper tracks to each other, but there is some randomness. By simulating the electric field distribution of PCB conformal coating surface dents and bumps, it is obtained that the existence of bumps or dents on the conformal coating surface can cause the electric field to be distorted and increased, which makes the PD breakdown path appear a certain randomness. In addition, it is observed that the accumulation of impurities on the PCB surface during the PD aging process may also be one of the reasons affecting the breakdown path.

The optical characteristics of the entire process for the PCB PD under square wave voltage from initiation to breakdown are studied in this article, which provides an important basis for the insulation design and fault diagnosis of PCB equipment in MEA.

References

[1] V. Madonna, P. Giangrande, W. Zhao, H. Zhang, C. Gerada, and M. Galea, "Electrical machines for the more electric aircraft: Partial discharges investigation," *IEEE Trans. Ind. Appl.*, vol. 57, no. 2, pp. 1389–1398, Mar. 2021.

[2] T. C. Cano et al., "Future of electrical aircraft energy power systems: An architecture review," *IEEE Trans. Transport. Electrific.*, vol. 7, no. 3, pp. 1915–1929, Sep. 2021.

[3] M. T. Fard, J. He, H. Huang, and Y. Cao, "Aircraft distributed electric propulsion technologies—A review," *IEEE Trans. Transport. Electrific.*, vol. 8, no. 4, pp. 4067–4090, Dec. 2022.

[4] Y. Zang et al., "Optical detection method for partial discharge of printed circuit boards in electrified aircraft under various pressures and voltages," *IEEE Trans. Transport. Electrific.*, vol. 8, no. 4, pp. 4668–4677, Dec. 2022.

[5] V. Madonna, P. Giangrande, and M. Galea, "Electrical power generation in aircraft: Review, challenges, and opportunities," *IEEE Trans. Transport. Electrific.*, vol. 4, no. 3, pp. 646–659, Sep. 2018.

[6] C. Emersic, R. Lowndes, I. Cotton, S. Rowland, and R. Freer, "Observations of breakdown through printed circuit board polymer coatings via a surface pollution layer," *IEEE Trans. Dielectr. Electr. Insul.*, vol. 24, no. 4, pp. 2570–2578, 2017.

[7] Y. Zang et al., "Partial discharge behavior of typical defects in power equipment under multilevel staircase voltage," *IEEE Trans. Dielectr. Electr. Insul.*, vol. 29, no. 4, pp. 1563–1573, Aug. 2022.

[8] J. Jiang, B. Zhang, Z. Li, C. Zhang, P. Ranjan, and X. Zhang, "Partial discharge investigation under low air pressure and variable frequency for more-electric-aircraft," *IEEE Trans. Dielectr. Electr. Insul.*, vol. 28, no. 5, pp. 1793–1801, Oct. 2021.

[9] H. Schefer, L. Fauth, T. H. Kopp, R. Mallwitz, J. Friebe, and M. Kurrat, "Discussion on electric power supply systems for all electric aircraft," *IEEE Access*, vol. 8, pp. 84188–84216, 2020.

[10] M. Borghei and M. Ghassemi, "Separation and classification of corona discharges under low pressures based on deep learning method," *IEEE Trans. Dielectr. Electr. Insul.*, vol. 29, no. 1, pp. 319–326, Feb. 2022.

[11] Q. Zhou et al., "Study on insulation breakdown characteristics of printed circuit board under continuous square impulse voltage," *Energies*, vol. 11, no. 11, p. 2908, Oct. 2018.

[12] S. Yamada, K. Okamoto, and K. Haga, "AC and impulse breakdown of polluted surface on printed wiring board," in *Proc. Electr. Insul. Conf. Electr. Manuf. Coil Winding Conf.*, 1997, pp. 9–805.

[13] G. Meng, Y. Cheng, J. Song, Y. Liu, K. Wu, and J. Dong, "Breakdown characteristics of PCB paralleled traces injected by rectangular pulse," in *Proc. Int. Symp. Electr. Insulating Mater.*, Sep. 2011, pp. 144–147.

[14] C. Emersic, R. Lowndes, I. Cotton, S. Rowland, and R. Freer, "The effects of pressure and temperature on partial discharge degradation of silicone conformai coatings," *IEEE Trans. Dielectr. Electr. Insul.*, vol. 24, no. 5, pp. 2986–2994, Oct. 2017.

[15] C. Abadie, T. Billard, S. Dinculescu, and T. Lebey, "On-line non intrusive PDs' measurements on aeronautical systems," in *Proc. Int. Symp. Electr. Insulating Mater. (ISEIM)*, vol. 1, Sep. 2017, pp. 99–103.
[16] Y. Wang et al., "Partial discharge investigation of form-wound electric machine winding for electric aircraft propulsion," *IEEE Trans. Transport. Electrific.*, vol. 7, no. 1, pp. 78–90, Mar. 2021.
[17] J. Jiang et al., "Optical sensing of partial discharge in more electric aircraft," *IEEE Sensors J.*, vol. 20, no. 21, pp. 12723–12731, Nov. 2020.
[18] N. Wiegart et al., "Inhomogeneous field breakdown in GIS–The prediction of breakdown probabilities and voltages. III. discharge development in SF_6 and computer model of breakdown," *IEEE Trans. Power Del.*, vol. 3, no. 3, pp. 939–946, Jul. 1988.
[19] Z. Guo, A. Q. Huang, and R. E. Hebner, "Characterization of partial discharges in high-frequency transformer under PWM pulses," *IEEE Trans. Power Electron.*, vol. 37, no. 9, pp. 11199–11208, Jun. 2022.
[20] P. H. F. Morshuis and F. H. Kreuger, "Transition from streamer to Townsend mechanisms in dielectric voids," *J. Phys. D, Appl. Phys.*, vol. 23, no. 12, pp. 1562–1568, Dec. 1990.
[21] N. Hayakawa, F. Shimizu, and H. Okubo, "Estimation of partial discharge inception voltage of magnet wires under inverter surge voltage by volume-time theory," *IEEE Trans. Dielectr. Electr. Insul.*, vol. 19, no. 2, pp. 550–557, Apr. 2012.
[22] C. Emersic and I. Cotton, "Experimental comparison of partial discharge between fast-switching pulse waves and square waves," *J. Phys. D, Appl. Phys.*, vol. 55, no. 38, Sep. 2022, Art. no. 385502.
[23] K. Maeda et al., "Partial discharge inception voltage of enameled cellular wire under impulse voltage," in *Proc. IEEE 2nd Int. Conf. Dielectr. (ICD)*, Jul. 2018, pp. 1–6.
[24] W. S. Zaengl, S. Yimvuthikul, and G. Friedrich, "The temperature dependence of homogeneous field breakdown in synthetic air," *IEEE Trans. Electr. Insul.*, vol. 26, no. 3, pp. 380–390, Jun. 1991.
[25] W. Song et al., "Aging characterization of high temperature vulcanized silicone rubber housing material used for outdoor insulation," *IEEE Trans. Dielectr. Electr. Insul.*, vol. 22, no. 2, pp. 961–969, Apr. 2015.
[26] P. Fu, Z. Zhao, X. Li, X. Cui, and Z. Yang, "The role of time-lag in the surface discharge inception under positive repetitive pulse voltage," *Phys. Plasmas*, vol. 25, no. 9, Sep. 2018, Art. no. 093518.

Yiming Zang was born in Shandong, China, in 1996. He received the B.E. degree in electrical engineering from Southwest Jiao Tong University, Chengdu, China, in 2018, and the Ph.D. degree in electrical engineering from Shanghai Jiao Tong University, Shanghai, China, 2022.

He is currently an Assistant Research Fellow with the School of Electrical Engineering, Shanghai Jiao Tong University. His research interests include online monitoring and fault diagnosis for power equipment insulation.

Mohamad Ghaffarian Niasar (Member, IEEE) was born in Tehran, Iran, in 1984. He received the M.Sc. degree from the Sharif University of Technology, Tehran, Iran, in 2008, and the Ph.D. degree in electrical engineering from the KTH Royal Institute of Technology, Stockholm, Sweden, 2015.

He is currently an Assistant Professor at the DC System, Energy Conversion and Storage Group, Technical University of Delft, Delft, The Netherlands. His main research interests are aging of electrical insulation, HVDC insulation system, partial discharges, high-frequency power transformers, power cables, and FEM modeling.

Yongpeng Xu received the Ph.D. degree from Shanghai Jiao Tong University, Shanghai, China, in 2018.

He is currently an Assistant Research Fellow with Shanghai Jiao Tong University. His research interests include intelligent monitoring technology of power equipment.

Ze Li was born in Shandong, China, in 1997. She received the B.E. degree in electrical engineering from North China Electric Power University, Baoding, China, in 2019. She is currently pursuing the Ph.D. degree in electrical engineering with Shanghai Jiao Tong University, Shanghai, China.

Her research interests include optical detection and fault diagnosis of partial discharge.

Qinglin Qian received the master's degree from Shandong University, Jinan, China, in 2013. He is currently pursuing the Ph.D. degree with Shanghai Jiao Tong University, Shanghai, China.

His research interests include online monitoring of power equipment.

Xiuchen Jiang was born in Shandong, China, in 1965. He received the B.E. degree in electrical engineering from Shanghai Jiao Tong University, Shanghai, China, in 1987, the M.S. degree in high voltage and insulation technology from Tsinghua University, Beijing, China, in 1992, and the Ph.D. degree in electrical engineering from Shanghai Jiao Tong University in 2001.

He is currently a Professor with the Department of Electrical Engineering, Shanghai Jiao Tong University. His research interests include online monitoring, condition-based maintenance, and automation for electrical equipment.

Peter Vaessen (Member, IEEE) was born in Maasbree, The Netherlands, in 1960. He received the M.Sc. degree (cum laude) in electrical power engineering from Eindhoven Technical University, Eindhoven, The Netherlands, in 1985.

In 1985, he joined KEMA (now a CESI brand). In his 35-year career, he held research positions in the field of large power transformers and high-voltage measurement and testing. He is a Manager of Innovations at KEMA Laboratories, Arnhem, The Netherlands, and the Chairperson of the European Distributed Energy Resources Laboratories Association (DERlab), Kassel, Germany, as well as a member of several national and international working groups. Since 2017, he has been a part-time Professor of hybrid transmission systems at TU Delft, Delft, The Netherlands, where he teaches high-voltage technology and HVDC.